Enhanced fast inertial relaxation engine (FIRE) for multiscale simulations

Tang, Mingjian; Shuang, Fei; Xiao, Pan

DOI
10.1016/j.commatsci.2024.113234

Publication date
2024

Document Version
Final published version

Published in
Computational Materials Science

Computational Materials Science 244 (2024) 113234

Contents lists available at ScienceDirect

Computational Materials Science

journal homepage: www.elsevier.com/locate/commatsci

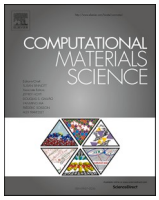

Full Length Article

Enhanced fast inertial relaxation engine (FIRE) for multiscale simulations

Mingjian Tang [a,b], Fei Shuang [c], Pan Xiao [a,*]

[a] LNM, Institute of Mechanics, Chinese Academy of Sciences, Beijing 100190, China
[b] School of Engineering Sciences, University of Chinese Academy of Sciences, Beijing 100049, China
[c] Department of Materials Science and Engineering, Faculty of Mechanical Engineering, Delft University of Technology, Mekelweg 2, Delft, 2628 CD, The Netherlands

ARTICLE INFO

Keywords:
Multiscale structural relaxation
Fast inertial relaxation engine
Atomistic to continuum coupling

ABSTRACT

In multiscale modeling methods (MMM), the integration of atomistic to continuum coupling is a common practice, where two regions have their own distinct length scales. The equilibrium configurations of such multiscale systems under given conditions are typically obtained through energy minimization algorithms (EMA). However, traditional EMAs, such as the conjugate gradient (CG) and limited-memory Broyden-Fletcher-Goldfarb-Shanno (LBFGS) algorithms, are unable to discern the diverse scales inherent in such systems. In this work, it is found that the convergence rate of energy minimization in multiscale simulations is significantly slower than that in full atomistic simulations, regardless of using CG, LBFGS algorithms or the latest fast inertial relaxation engine (FIRE). The lower efficiency emerges due to the coexistence of atoms and nodes with distinct length scales within the multiscale framework, yet the current EMAs fail to differentiate between them. It results in disparate convergence rates across different scales, which undermines both computational accuracy and efficiency. To address the issue, a multiscale FIRE algorithm which updates positions of atoms and nodes synchronously by employing appropriate effective mass is proposed. The optimal effective mass is determined by synchronizing the vibration of harmonic oscillators across different scales. By employing the multiscale FIRE algorithm, the computational efficiency increased by 24.4 and 23.7 times compared to the CG and LBFGS algorithms when used for multiscale nanoindentation simulations. These findings and the proposed algorithm provide valuable insights for structural relaxations of multiscale physical problems and are promising to further improve the computational accuracy and efficiency of MMMs.

1. Introduction

The past few decades have witnessed numerous research progress made on the concurrent multiscale modeling methods (MMM) with atomistic to continuum coupling [1,2], which can significantly enhance computational efficiency while preserving accuracy. The simulation methods at the micro-scale, represented by molecular dynamics (MD) and molecular statics (MS), can predict the behavior of materials at atomic level, yet they are limited to small spatial and temporal scales, typically ~ 100 nm and ~ 10 ns, because of their high computational consumption [3]. On the other hand, the computational methods at the macro-scale, such as finite element method (FEM) and phase-field method, can deal with large-scale systems but struggle with simulating inhomogeneous deformation at atomic level. Therefore, MMMs are proposed to integrate atomistic and continuum representations within the same system in order to balance accuracy and efficiency [4,5]. Among the proposed MMMs, the quasicontinuum (QC) method developed by Tadmor et al. [6] is one of the representative methods. By introducing representative atoms for mesh interpolation in non-critical regions, QC significantly reduces the degrees of freedom (DOF). Cauchy-Born rule is applied to approximate the energy of the system, which further improves the computational efficiency. On this basis, extensive research efforts have been dedicated to improving QC, for instance, by introducing adaptivity [7,8], correcting ghost force at interfaces [9,10], and considering finite temperature effect [11,12]. So far, QC has been used to solve many mechanical problems, such as nanovoids [8], interfacial motion of crystals and crack propagations [13,14]. The coupled atomistic and discrete dislocation (CADD) method [15,16] is an extension of QC, where the discrete dislocation lines are introduced to represent dislocations in elements, and it is not required to conduct transformation between atomistic and continuum regions in CADD. With the decomposition of the displacement field, the bridging scale method (BSM) [17–19] establishes the coupling of macro-scale and micro-scale, and is suitable for both static and dynamic problems, such

* Corresponding author.
E-mail address: xiaopan@lnm.imech.ac.cn (P. Xiao).

https://doi.org/10.1016/j.commatsci.2024.113234
Received 7 June 2024; Received in revised form 9 July 2024; Accepted 10 July 2024
Available online 23 July 2024

as deformation of carbon nanotubes and 2D wave conduction. Budarapu et al. [20] has put forward a multiscale method for quasi-static crack propagation simulations. In this method, the classical MS and a coarse-grained model with virtual atom clusters are used for atomistic and continuum regions respectively, and the phantom node method is adopted when an element is cut by a crack. With the coupling of MD and smoothed molecular dynamics (SMD), Liu et al. [21] put forward a concurrent multiscale method to solve the problem of limited temporal and spatial scales in MD simulations at finite temperature. With a two-level description of the lattice structure and the extended transport equations, Chen et al. [22] proposed the concurrent atomistic-continuum (CAC) method, which allows the propagations of dislocations through coarse-grained elements without switching them into atomic representations. Notably, Wang et al. [23] proposed the molecule/cluster statistical thermodynamics (MCST) multiscale framework, which solves the equilibrium configuration of the finite temperature system by minimizing its Helmholtz free energy. In this framework, the molecule statistical thermodynamics (MST) [24], cluster statistical thermodynamics (CST) [25] and hybrid molecule/cluster statistical thermodynamics (HMCST) methods can be used to calculate the quasi-static mechanical behaviors and have been applied to mechanical analysis of both 2D and 3D systems at finite temperature [26].

For these MMMs, it is an important issue to achieve high computational efficiency while maintaining accuracy. Previous studies have examined the efficiency of some MMMs, demonstrating their superior performance compared with full atomistic simulations. For example, Biyikli et al. [27] put forward the multiresolution molecular mechanics used for a nanoindentation problem, which shows 6.3 ~ 8.5 times higher than MD in efficiency. The variable node multiscale method [28], coupling FEM and classical MS with decomposition of displacement into coarse and fine scales, reduces 4.4 times of computational time than pure MS in simulating a 2D edge crack problem. A coupling extended multiscale finite element and peridynamic method proposed by Zhang et al. [29] was used for simulations of the quasi-static crack propagations, and its calculation time for each loading step was 119.2 s, while that of the peridynamic method was 876.7 s.

Generally speaking, the efficiency of an MMM for quasi-static simulations is related to two aspects: the coupling algorithm across different scales and the efficiency of the energy minimization algorithm (EMA). Since the coupling algorithm varies across different MMMs for specific applications, developing efficient EAMs for multiscale simulations can benefit all MMMs. Currently, classical EMAs, such as the conjugate gradient (CG) and limited-memory Broyden-Fletcher-Goldfarb-Shanno (LBFGS) algorithms, have been widely used. These EMAs are renowned for their reliability and efficiency in tackling a wide range of minimization problems, owing to extensive studies in the mathematical optimization community [30]. In order to further improve the efficiency of energy minimization for atomic systems, Bitzek et al. [31] proposed the fast inertial relaxation engine (FIRE) algorithm which shows great efficiency improvement than CG. However, the original FIRE has several aspects that could be further improved. For example, based on structural relaxation in the microcanonical (NVE) ensemble, Lin et al. [32] proposed a new EMA applied to indentation on monolayer graphene, consuming less computational time than CG and FIRE algorithms. Zhou et al. [33] put forward a mass-weighted FIRE algorithm for the Green's function molecular dynamics, which shows about 3 times higher than CG and the initial FIRE in computational efficiency when applied to the problem of Hertzian contact. Guénolé et al. [34] proposed the FIRE 2.0 algorithm with corrected iterations and uphill motion, which shows better robustness than the initial FIRE and higher efficiency than CG when used for numerical examples such as dislocation relaxation and energy barrier calculations. Currently, the FIRE algorithm has been integrated into most popular atomic/molecular simulation packages, such as LAMMPS [35], VASP [36], IMD [37] and GROMACS [38].

However, the convergence behavior of the FIRE algorithm in multiscale simulations remains unclear. In a full atomistic system, the existing EMAs determine proper magnitudes and directions for all DOFs for the next move based on the current state of energy and force. For the atomistic to continuum coupling MMMs, atoms and nodes are usually treated equally by current EMAs, such that their step sizes are taken as the same value at each iteration step. However, it may prove inefficient in practice because the convergence rates of atomistic and continuum regions could differ significantly due to their different characteristic length scales, as observed in the current study. If the same step size is adopted for atoms and nodes, the converged rates of atomistic and continuum regions may not be consistent, thereby compromising computational efficiency. Despite some previous research [39] comparing the computational efficiency of different EMAs for MMMs, little literature has addressed the underlying reasons for this problem of efficiency and put forward corresponding solutions.

In this work, typical EMAs will be applied to an MMM to investigate the effects of atomistic to continuum coupling on the efficiency and accuracy for energy minimization. Subsequently, an improved FIRE algorithm will be proposed to achieve higher efficiency for MMMs and offer insights for improving the optimization of other multiscale models. The multiscale framework MCST [23] will be used to validate the efficiency of EMAs. In Section 2, the MCST will be briefly reviewed at first, and the essentials of FIRE algorithm will be discussed. In Section 3, the 3D nanoindentation will be used as numerical examples to indicate the efficiency problems of EMAs involved in the energy minimization of multi-scale simulations. On this issue, the multiscale FIRE algorithm is proposed in Section 4 and its efficiency and accuracy will be verified in Section 5. Finally we will summarize our work and its significance to general multiscale problems in Section 6 and 7.

2. MCST multiscale framework and energy minimization

In previous studies, Wang et al. [23] proposed the MCST framework for simulations with atomistic to continuum coupling. Depending on different representation styles, MCST can be used in three computational modes: the MST method [24] with atomistic representation, the CST method [25] with continuum representation, and the HMCST method which combines both representations, as shown in Fig. 1. In all the computational modes, mechanical behavior of a solid system can be obtained by minimization of the total energy.

The MST method was developed for quasi-static simulations of finite temperature systems. By incorporating the local harmonic approximation [40] into the Helmholtz free energy, the temperature effect could be considered without calculating atomic thermal vibrations. MST can accurately capture inhomogeneous deformation such as cracks and dislocations, yet its computational cost is huge because the motion of each atom should be traced. The CST method was put forward as a "coarse-grained" version of MST to reduce the DOFs. CST divides the system into several clusters, where the atoms are evenly distributed, and their positions could be determined by nodes. While CST offers significantly higher efficiency than MST, it is difficult to model atomic motions in regions with local defects. In order to balance both computational accuracy and efficiency, the HMCST method was designed by combining MST and CST. As illustrated in Fig. 1, a system is divided into the molecule and cluster regions, where energy calculations are performed using the MST and CST methods respectively. Additionally, padding atoms are introduced in the cluster regions to compute the interatomic interactions with adjacent molecule regions. As a result, the total free energy of the system comprises the following three parts:

$$E^{\mathrm{tot}} = E^{\mathrm{M}}(\{\mathbf{x}_{atom}\}) + E^{\mathrm{C}}(\{\mathbf{X}_{node}\}) + E^{\mathrm{I}}(\{\mathbf{x}_{atom}\},\{\mathbf{X}_{node}\}) \tag{1}$$

where E^{M}, E^{C}, E^{I} are the free energy of molecule, cluster and interfaces respectively; $\{\mathbf{x}_{atom}\}$ and $\{\mathbf{X}_{node}\}$ represent the sets of coordinates of atoms and nodes. Moreover, the adaptive HMCST has the ability to switch cluster regions to molecule regions adaptively when defects in the molecule region are going to propagate across the interface of the

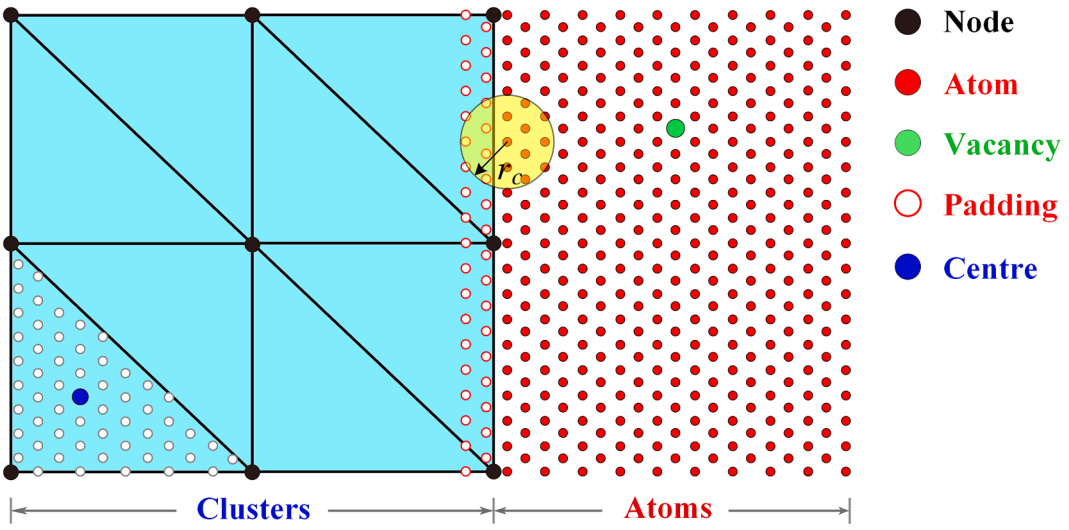

Fig. 1. Schematic illustration of the HMCST method.

two regions.

In both MST and HMCST methods, the quasi-static mechanical response of the system is determined by the energy minimization. For this purpose, CG, LBFGS and FIRE algorithms are three of most commonly used EMAs as introduced in Section 1. This study mainly focus on the FIRE algorithm, while the results obtained with CG and LBFGS will be used for comparison in Section 3.

Unlike CG and LBFGS where the step size is determined by the line search, the FIRE algorithm proposed by Bitzek et al. [31] updates the coordinates of DOFs by means of an MD-like integration method with a damping coefficient. In this study, we employ the semi-implicit Euler integration method, in which the velocity and coordinates are updated as follows:

$$\mathbf{v}^{(k+1)} = \mathbf{v}^{(k)} + \frac{\mathbf{f}^{(k)}}{m}\Delta t, \mathbf{x}^{(k+1)} = \mathbf{x}^{(k)} + \mathbf{v}^{(k+1)}\Delta t \tag{2}$$

where Δt represents the time step and m denotes the mass of particles.

To enhance the robustness of FIRE, we adopt the FIRE 2.0 algorithm [34] mentioned in Section 1, and its computational process for the HMCST method which couples atomistic and continuum representations is detailed in Appendix A.

For the FIRE algorithm, achieving convergence mainly relies on two essential parameters in Eq. (2): the initial time step and masses of particles. Typically, the time step is set to be equal for atoms and nodes. Regarding the masses of atoms and nodes, there are two common strategies: (1) both the masses of atoms and nodes are set to the physical mass of the atoms; (2) the mass of nodes is set to be the summation of the mass of their representative atoms according to the approach of coarse-graining [41]. Compared with the first strategy, it makes more sense in terms of dynamics when aligning the mass of nodes to their representative atoms. However, the numerical simulations in Sections 3 and 5 will indicate that neither approach achieves the optimal convergence rate.

3. Efficiency analysis of multiscale simulations with different EMAs

As a typical multiscale problem in computational mechanics, nanoindentation has been commonly used to validate the feasibility and efficiency of MMMs [27,42,43]. The nanoindentation system is consisted with an indenter and substrate, made from a specific material to be tested. In practice, the indenter is pressed into the substrate with a displacement load, establishing the relationship between the indentation depth and reaction force that reflects the mechanical properties of the substrate. In crystalline materials, dislocations will nucleate beneath the indenter as the applied load increases and gradually propagate into the substrate. Therefore, in the multiscale simulation of the nanoindentation system, atomistic representation regions are used to capture the nucleation and propagation of dislocations, while the continuum representation regions describe the elastic deformation away from dislocations in order to reduce computational DOFs.

In this Section, the MST and adaptive HMCST methods with the CG, LBFGS and FIRE algorithms are used to simulate a nanoindentation system as illustrated in Fig. 2. The substrate is consisted of a single crystal copper with a dimension of 39.0 × 39.0 × 27.5 nm, containing 3,602,309 Cu atoms. The lattice structure of the substrate is face-centered cubic (FCC), with the lattice constant of 3.615 Å and the indented surface is (001). The conical diamond indenter contains 25,984C atoms, with the lattice constant of 3.567 Å and the cone angle of 120 degrees. During the quasi-static loading process, the indenter moves downward to a maximum depth of 3.6 nm with 200 loading steps. In the system for MST simulations as shown in Fig. 2 (a), 348,074 atoms are fixed at the bottom of the substrate, while periodic boundary conditions are applied to the x and y directions. The embedded-atom method (EAM) potential [44] is adopted to describe the interactions of Cu atoms. While the potential energy between C and Cu atoms are calculated by the Morse potential $\phi_{\mathrm{C-Cu}}(r) = D_0\left[\left(1 - e^{-\alpha(r-r_0)}\right)^2 - 1\right]$, where the parameters$D_0 = 0.087$ eV, $\alpha = 5.14$ Å^{-1} and$r_0 = 2.05$ Å [24] are used, and the cutoff radius is set to 7.0 Å for the C-Cu atomic interactions. Here the temperature effect is not considered in the simulations, and the Helmholtz free energy is equal to the interatomic potential energy. Therefore, the MST method is equivalent to the classical MS in this case, which will be used as the benchmark in the comparison with the adaptive HMCST method.

In the initial configuration for the adaptive HMCST simulations as shown in Fig. 2 (b), the top surface of the substrate with a thickness of 1.1 nm containing 117,723 atoms is set as the molecule region used for the generation of initial defects. The initial cluster region consists of 2,916 tetrahedral elements with 700 nodes. Its boundary condition is similar to that of MST, except that 100 nodes are fixed at the bottom.

The same convergence criterion of force is adopted for CG, LBFGS and FIRE algorithms in order to compare their computational efficiency and accuracy. Specifically, the magnitude of the forces of all atoms in the system is employed as a measure to check the convergence state, which is defined as:

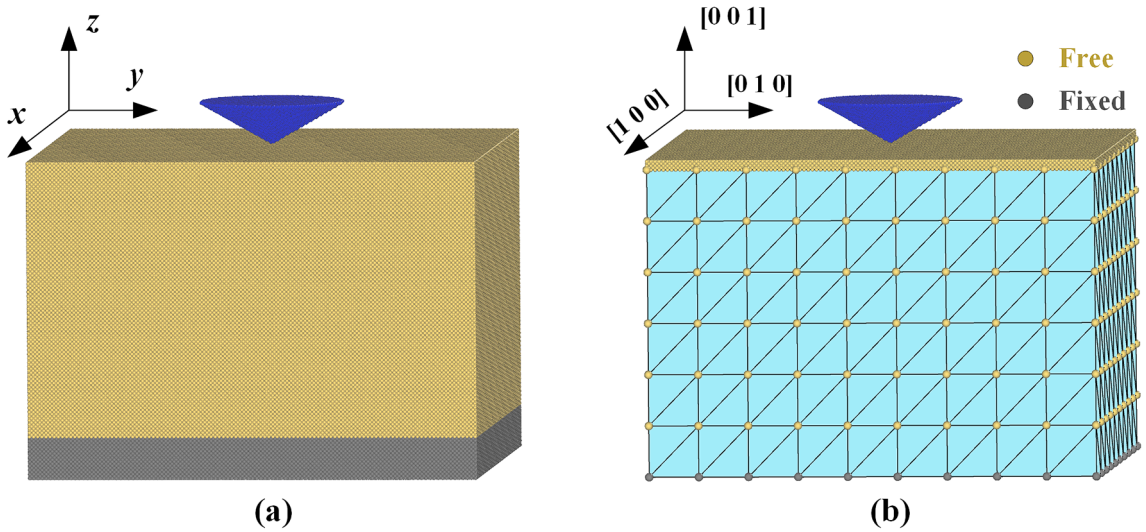

Fig. 2. Nanoindentation configurations for the (a) MST and (b) adaptive HMCST simulations.

$$\bar{f} = \sqrt{\frac{1}{N_{total\_atoms}}\left(\sum_{atom}\mathbf{f}_{atom}\cdot\mathbf{f}_{atom} + \sum_{node}\mathbf{F}_{node}\cdot\mathbf{F}_{node}\right)} < \varepsilon_{\bar{f}} \tag{3}$$

where $\mathbf{f}_{atom}$, $\mathbf{F}_{node}$ represent the force vectors of atoms and nodes; N_{total_atoms} refers to the total number of atoms in the simulated system, including the virtual atoms in cluster regions; $\varepsilon_{\bar{f}}$ is the converged threshold, which is set as 5.0e-4 eV/Å for all the considered methods. In addition, for the adaptive HMCST simulations with the FIRE algorithm, two different masses of nodes as mentioned in Section 2 are both tested: (1) m_{node}=m_{atom}; (2)m_{node} = 4978 m_{atom}, where 4978 refers to the average number of representative atoms of nodes in the cluster regions of the multiscale system.

Fig. 3 shows the dislocation pattern of the nanoindentation systems at the last loading step from the MST and adaptive HMCST methods, rendered with the centrosymmetric parameters (CSP) [45] ranging between 1.0 and 6.5 Å^2. Here the results are computed with the FIRE algorithm. It can be observed that both the calculated results of MST and HMCST have significant dislocations generated around the indenter. In the case when m_{node}=m_{atom}, there are few dislocation loops extend into the interior of the substrate as shown in Fig. 3 (b) compared with the MST. Fig. 3 (c) corresponds to the results whenm_{node} = 4978 m_{atom}, showing that some dislocation loops extend towards the boundary of the substrate, which are closer to the results of MST in Fig. 3 (a). On this issue, we will further analyze from the aspects of the force-depth curves and the iteration processes of forces in molecule and cluster regions.

Fig. 4 shows the force-depth curves obtained from the MST and adaptive HMCST simulations with three different EMAs. For the same method, the curves obtained by CG, LBFGS and FIRE algorithms are similar, where some differences are due to the random development of dislocations. the To make quantitative comparison, quadratic functions were employed for fitting these force-depth curves, and the fitting coefficients obtained from the MST and HMCST with CG, LBFGS and FIRE (m_{node}=m_{atom}) algorithms are 114.1, 106.7, 114.9 and 129.8, 128.2, 134.0 nN/nm^2 respectively. HMCST produces results that exhibit a slightly higher stiffness of the system compared to MST. For the FIRE algorithm, the fitting coefficients from the results of MST and HMCST whenm_{node} = m_{atom}andm_{node} = 4978 m_{atom} are 114.9, 134.0 and 102.4 nN/nm^2 respectively. It is indicated that the results of adaptive HMCST exhibit discrepancies compared to the MST used as the benchmark. Notably, the stiffness of the force-depth curve by HMCST-FIRE whenm_{node} = 4978 m_{atom} is significantly lower than other HMCST results but comparable to MST results. These comparisons indicate that FIRE withm_{node} = 4978 m_{atom} is the most physical EMA by considering the coarse-grained mass of nodes and has the best accuracy.

The computational efficiency of the MST and adaptive HMCST methods employing three EMAs are presented in Table 1. Here we compare the number of force and energy evaluations n_{FE} for different computational conditions. Several distinct characteristics can be observed from these results.

The computational time of MST and HMCST simulations is not directly compared here, primarily because the calculation cost of each force/energy evaluation differs significantly between full

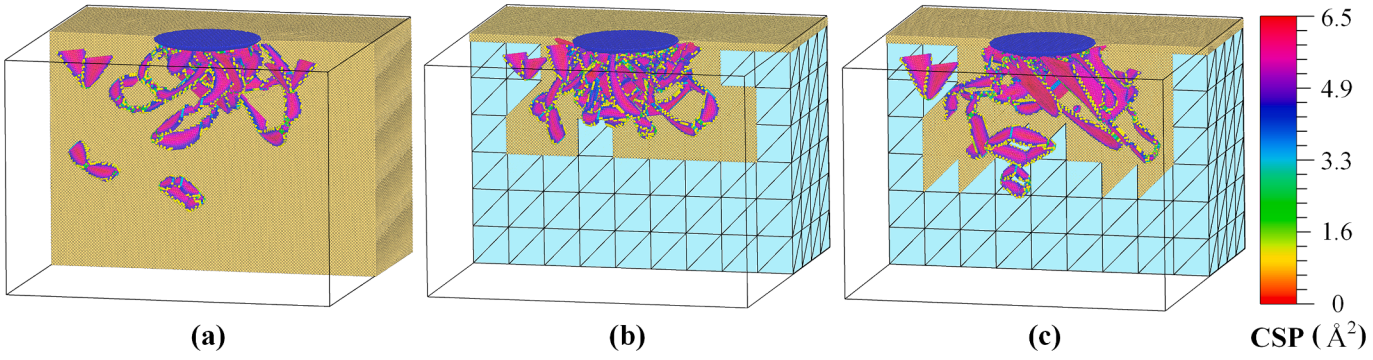

Fig. 3. Dislocation distributions in the nanoindentation systems at the maximum indentation depth obtained from the (a) MST and adaptive HMCST simulations with the FIRE algorithm when (b)m_{node} = $m_{atom}$and (c)m_{node} = 4978 m_{atom} in a semi-sectional style.

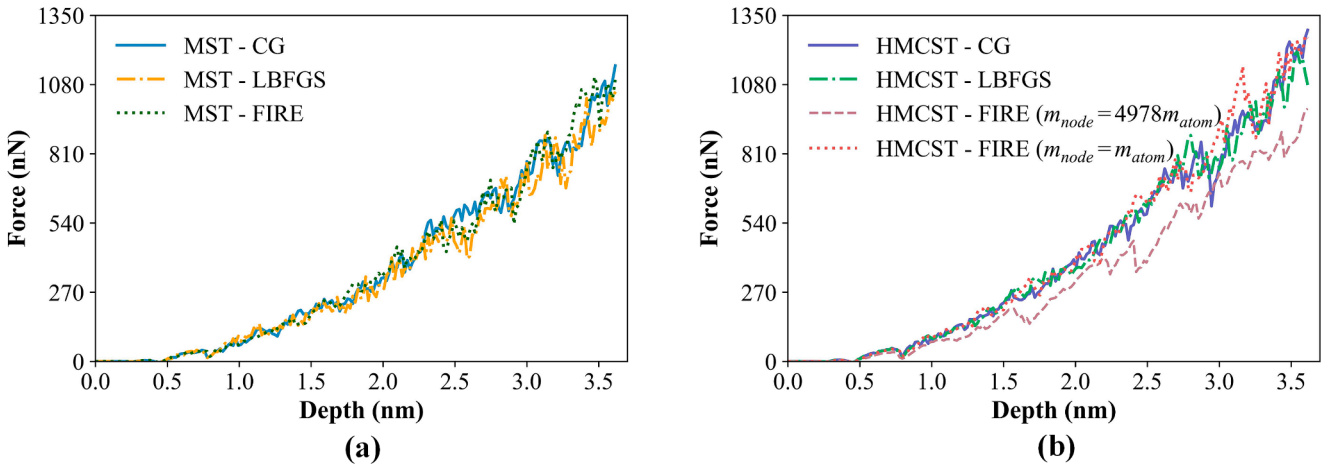

Fig. 4. Force-depth curves obtained by the (a) MST and (b) adaptive HMCST methods with CG, LBFGS and FIRE algorithms.

Table 1
Number of force evaluations of MST and adaptive HMCST by CG, LBFGS, original and multiscale FIRE algorithms.

Method		Number of force evaluations
Full atomistic	MST-CG	134,373
	MST-LBFGS	119,680
	MST-FIRE	30,109
Multiscale	HMCST-CG	666,151
	HMCST-LBFGS	628,096
	HMCST-FIRE (m_{node}=m_{atom})	281,390
	HMCST-FIRE (m_{node}=4978 m_{atom})	72,346
	HMCST-Multiscale FIRE	**27,160**

atomistic and multiscale models. The discrepancy arises from varying DOFs and parallel implementation, making it difficult to conduct fair comparison for the wall time of two systems. Moreover, the model of 3D nanoindentation is relatively small, diminishing the potential advantages of multiscale simulations. Therefore, we opt to compare the numbers of force evaluations, as this metric better demonstrates the convergence rate of the energy minimization process.

In both MST and HMCST simulations, different minimization algorithms exhibit similar characteristics of efficiency. The computational time for the CG algorithm is the longest, followed by the LBFGS algorithm, while the FIRE algorithm is the fastest. The result is consistent with the findings of the FIRE algorithm in other simulations as well [34,39]. To be more specific, considering the total number of force evaluations in the MST simulations, the LBFGS algorithm costs 89.1 % of the CG algorithm, and the FIRE algorithm is 4.5 times faster than the CG algorithm. In the adaptive HMCST simulations, the efficiency of the CG and LBFGS algorithms is close, and the FIRE algorithm with $m_{node} = m_{atom}$ and $m_{node} = 4978\ m_{atom}$ is 2.4 and 9.2 times faster than the CG algorithm respectively.

For the same minimization algorithm, both the total computation time and the number of force evaluations in HMCST simulations are higher than that in MST simulations. Specifically, the number of force evaluations in HMCST with the CG algorithm is 5.0 times that of the MST method, while with the LBFGS algorithm, it is 5.2 times that of the MST method. The number of force evaluations in HMCST using the FIRE algorithm in the cases of $m_{node} = m_{atom}$ and $m_{node} = 4978\ m_{atom}$ is 9.3 and 2.4 times that of the MST method respectively. These results indicate that although the HMCST method effectively reduces the DOFs by introducing clusters, the convergence rate is lower than the MST method with full atomistic representation.

In order to explain the underlying reason for the different accuracy in Fig. 4 (b) as well as low efficiency of multiscale simulations in Table 1, the forces of atoms and nodes in the molecule and cluster regions are recorded during the iteration process. Fig. 5 (a) and (b) show the average forces of atoms and nodes for the HMCST simulations at the indented depth of 2.2 nm and the FIRE algorithm when $m_{node} = m_{atom}$ and $m_{node} = 4978\ m_{atom}$. Here the average forces of atoms and nodes are calculated as $\bar{f}_{atom} = \sqrt{\frac{1}{N_{atom}}\sum_{atom}\mathbf{f}_{atom}\cdot\mathbf{f}_{atom}}$, $\bar{F}_{node} = \sqrt{\frac{1}{N_{node}}\sum_{node}\mathbf{F}_{node}\cdot\mathbf{F}_{node}}$, where N_{atom} and N_{node} represent the number of atoms molecule regions and nodes in the cluster regions, respectively. In the case that $m_{node} = m_{atom}$ as shown in Fig. 5 (a), $\bar{F}_{node}$ fluctuates violently during the energy minimization. However, the lowest $\bar{F}_{node}$ is one order magnitude smaller than $\bar{f}_{atom}$. In contrast, Fig. 5 (b) shows the iteration process of forces when $m_{node} = 4978\ m_{atom}$. Due to a larger mass of nodes, the fluctuations of $\bar{F}_{node}$ in Fig. 5 (b) are not considerable as that in Fig. 5 (a). Nevertheless, the value of $\bar{F}_{node}$ during iterations remain 10^{-1} nN, which is much higher than $\bar{f}_{atom}$ with a converged value of nearly 10^{-4} nN.

From Fig. 5, the following reasons can be inferred for the different accuracy and efficiency of HMCST simulations:

For FIRE with m_{node}=m_{atom}, Fig. 5 (a) indicates that the molecular regions are under-converged, while the cluster regions are over-converged. Although the criterion in Eq. (3) is satisfied at the end of minimization, this convergence is fake, and the energy of the multiscale system is not truly minimized. Since the molecule regions directly contact the indenter, the non-zero forces in these regions exert a high force on the indenter, leading to increased stiffness in the force-depth curve in Fig. 4 (b). This fake convergence also explains the high stiffness observed in the force-depth curves for HMCST-CG and HMCST-LBFGS in Fig. 4 (b).

On the contrary, Fig. 5 (b) suggests that the molecule regions are over-converged, while the cluster regions are not fully relaxed eventually when $m_{node} = 4978\ m_{atom}$. As a consequence, the corresponding force-depth curve has lower stiffness, mainly due to the non-converged cluster regions, which are more "soft" compared with other curves. Nevertheless, the highly converged molecule regions enable the accurate dislocation evolution and force-depth curve, as shown in Fig. 3 (c) and Fig. 4 (b).

The convergence rates of molecule and cluster regions are distinct in both Fig. 5 (a) and (b). The different convergence rates of two regions lead to twists and turns in the energy minimization process, resulting in low efficiency of multiscale simulations.

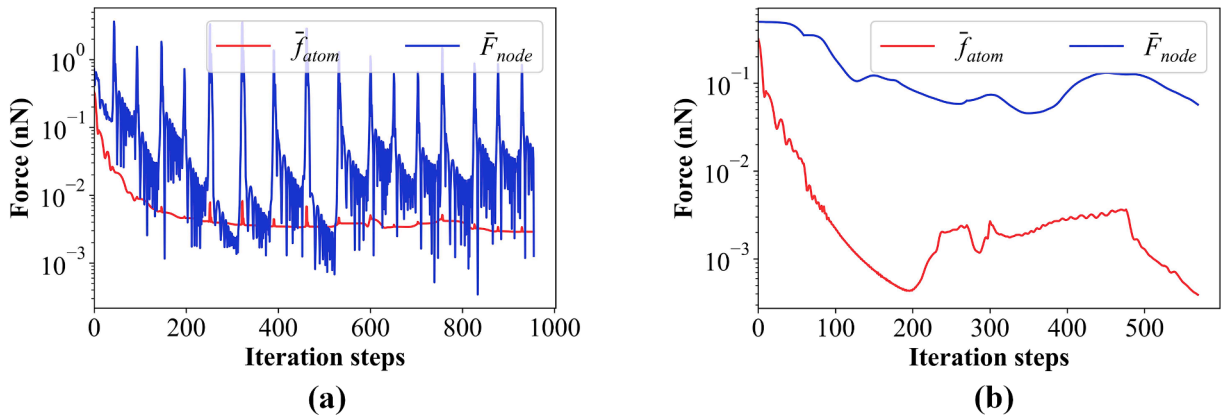

Fig. 5. Average forces of atoms and nodes for the adaptive HMCST simulations with the original FIRE algorithm when (a) m_{node}=m_{atom}, (b)m_{node} = 4978 m_{atom} during the iteration process at the indented depth of 2.2 nm.

4. FIRE algorithm for multiscale simulations

According to the results in Section 3, the computational efficiency of EMAs in HMCST is lower than that for MST, primarily due to the different convergence rates of molecule and cluster regions. Compared with the CG and LBFGS, the FIRE algorithm not only exhibits higher efficiency, but also offers clearer physical and dynamic interpretations. Therefore, a multiscale FIRE algorithm will be proposed to address this issue. Specifically, we will discuss the relationship between system's energy and masses and oscillation frequencies during energy minimization, and analyze the effective mass of nodes in physical systems.

4.1. Relationship of masses and oscillation frequencies in energy minimization

The potential energy of a system with a total number of atoms and nodes as N_{total} can be calculated through the Taylor's expansion near the equilibrium state:

$$\Phi = \Phi_0 + \sum_{i=1}^{N_{total}} \sum_{\alpha=1}^{3} \frac{\partial \Phi}{\partial r_{i\alpha}}\bigg|_{\mathbf{r_0}} \Delta r_{i\alpha} + \frac{1}{2} \sum_{i,j=1}^{N_{total}} \sum_{\alpha,\beta=1}^{3} \frac{\partial^2 \Phi}{\partial r_{i\alpha} \partial r_{j\beta}}\bigg|_{\mathbf{r_0}} \Delta r_{i\alpha} \Delta r_{j\beta} + \cdots \tag{4}$$

where Φ_0 corresponds to the potential energy at the reference point; $r_{i\alpha}$ represents the coordinate of ith atom or node on the αth direction; $\boldsymbol{r_0}$ refers to the coordinates of DOFs at the equilibrium state. Due to the fact that the force of DOFs equals zero at the equilibrium state, and by neglecting higher-order terms, the potential energy in Eq. (4) only retains Φ_0 and the terms with the second-order gradient. According to the dynamical theory of lattice, the second-order gradient of Φ can be expressed by the lattice dynamical matrix $\mathbf{D}$[46–48]. As a result, the potential energy can be written as:

$$\Phi = \Phi_0 + \frac{1}{2} \sum_{i,j=1}^{N_{total}} \sum_{\alpha,\beta=1}^{3} \sqrt{m_i m_j} D_{ij}^{\alpha\beta} \Delta r_{i\alpha} \Delta r_{j\beta} \tag{5}$$

where m_i represents the mass of ith atom or node. In order to simplify the analysis, both the local harmonic and decoupled approximations are applied, where the couplings of oscillations among and on different directions of atoms and nodes are neglected. Based on the relationship between oscillation frequencies and the lattice dynamical matrix, the potential energy could be calculated as follows:

$$\begin{aligned}\Phi &\approx \Phi_0 + \frac{1}{2} \sum_{i=1}^{N_{total}} \sum_{\alpha=1}^{3} m_i \omega_{i\alpha}^2 \Delta r_{i\alpha}^2 \\ &= \Phi_0 + \frac{1}{2} \sum_{i=1}^{N_{atom}} \sum_{\alpha=1}^{3} m_{atom,i} \omega_{atom,i\alpha}^2 \Delta r_{atom,i\alpha}^2 + \frac{1}{2} \sum_{i=1}^{N_{node}} \sum_{\alpha=1}^{3} m_{node,i} \omega_{node,i\alpha}^2 \Delta r_{node,i\alpha}^2\end{aligned} \tag{6}$$

where $\omega_{i\alpha}(\alpha = 1, 2, 3)$ represent oscillating frequencies of ith atom or node. Eq. (6) indicates that the system's energy can be divided into three contributions: ground state energy, vibrational energy of all atoms, and vibrational energy of all nodes. To achieve the optimal convergence rate when relaxing the system, atoms and nodes should move synchronously. Since vibrational frequency is an intrinsic property of the system determined by the predefined potential energy, m_{atom} and m_{node} can be adjusted accordingly.

To illustrate this point, the energy minimization of a 2D quadratic potential function $\Phi(x_1, x_2) = \frac{1}{2}k_1 x_1^2 + \frac{1}{2}k_2 x_2^2$ is calculated, where the resilience factors$k_1 = 2$ eV/Å^2, $k_2 = 20$ eV/ Å^2, and the initial value is (1 Å, 1 Å). Besides, the parameters$m = 10$ eV•fs^2/Å^2, $\Delta t_0 = 0.7$ fs are set for both x_1 and x_2 when using the FIRE algorithm. The whole minimization process is shown in Fig. 6 (a) and (b).

It is indicated from the results that the iteration process with the original FIRE algorithm encounters twists and turns. Obviously, the particle fluctuates violently on the direction of x_2 especially on the beginning few steps, while the convergence rate is relatively slow on the direction of x_1. Additionally, the DOF with a larger curvature of the potential well has larger oscillation frequencies than the one with a smaller curvature. When minimizing the energy of this system, it could be difficult for two DOFs to reach the equilibrium state simultaneously if their oscillation frequencies are distinct. As a result, it is difficult for the original FIRE to search a reasonable minimization path for the multiscale system.

Since the resilience factors for the ith atom or node defined as $k_{i\alpha} = m_i \omega_{i\alpha}^2$ could be obtained from the concrete potential function, and its oscillation frequencies are calculated by $\omega_{i\alpha} = \sqrt{k_{i\alpha}/m_i}$. Now the results after synchronizing the oscillations of x_1, x_2 will be calculated. For this purpose, we set$m_2 = 10\, m_1$, to make sure that the oscillation frequencies of two DOFs are the same. The FIRE algorithm with corrected masses of DOFs based on synchronizing their oscillation frequencies is referred to as the "multiscale FIRE algorithm". With the same parameters and initial value used above except for$m_2 = 10$ eV•fs^2/Å^2 and$m_1 = 1$ eV•fs^2/Å^2, the minimization process of $\Phi(x_1, x_2)$ with the multiscale FIRE algorithm is shown in Fig. 6 (c) and (d). It is observed that the results with multiscale FIRE could converge directly to the location nearby the exact solution (0 Å, 0 Å) without any twist or turn on one direction shown in Fig. 6 (b). Notably, the number of iteration steps that the multiscale FIRE

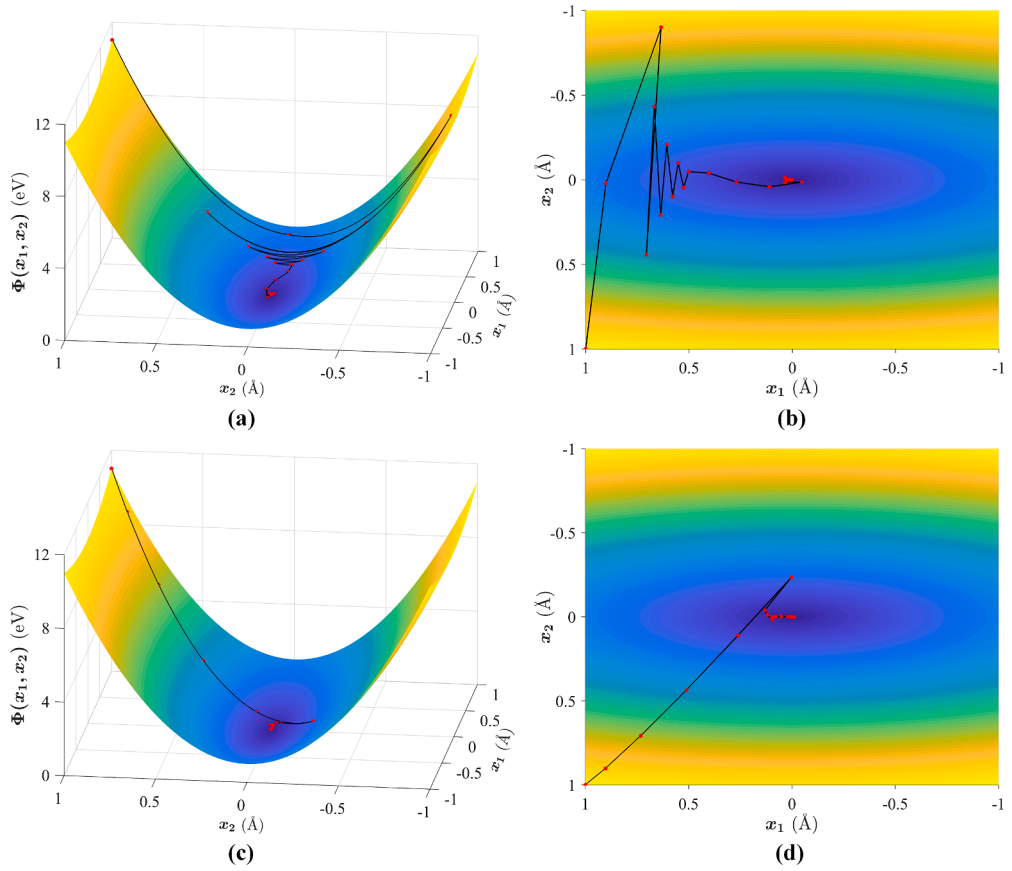

Fig. 6. Minimization process of a 2D quadratic potential function using the (a) (b) original FIRE and, (c) (d) multiscale FIRE algorithm.

consumes for the minimization of $\Phi(x_1, x_2)$ is 27, while the original FIRE costs 52 iteration steps. These results indicate that synchronizing the oscillation frequencies of DOFs across different scales can effectively accelerate the convergence rate of the minimization process.

4.2. Corrected effective mass of nodes

In this Subsection, we will determine the effective mass of nodes for the atomistic to continuum coupling MMMs by synchronizing the oscillation frequencies of atoms and nodes in Eq. (6).To simplify the analysis, the following three assumptions are introduced: (i) the interatomic interactions will occur only among the nearest neighbors of atoms instead of a larger range within a cut-off radius; (ii) the motion of atoms in the whole system could be approximated to the harmonic oscillators, so the interatomic forces are proportional to the distance from the equilibrium state; (iii) the length of elements in cluster regions is significantly larger than the interatomic distance. Based on these assumptions, we will analyze the effective mass of nodes for a practical 3D multiscale system.

As shown in Fig. 7, the lattice structure is FCC, with the cluster regions divided by tetrahedral elements. Notably, we take the directions parallel to the boundaries of the coupling interface as the x and y coordinates, while the vertical direction of the interface is regarded as the z coordinate. According to our assumptions, an effective spring oscillator model with a stiffness of k could be built between every two adjacent atoms. Suppose a disturbance Δx on the x direction is given to an atom in molecule regions, and the increase of energy could be calculated as follows:

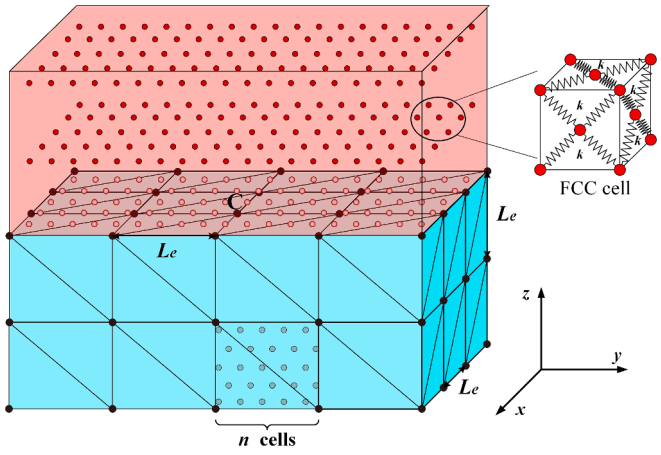

Fig. 7. Configuration of the 3D multiscale system.

$$\Delta E^{(x)}_{atom-3D} = 4 \times \frac{1}{2}k\left(l_0 + \frac{\sqrt{2}}{2}\Delta x\right)^2 + 4 \times \frac{1}{2}k\left(l_0 - \frac{\sqrt{2}}{2}\Delta x\right)^2 - 4 \times \frac{1}{2}kl_0^2 = 2k\Delta x^2 \tag{7}$$

where l_0 corresponds to the interatomic distance at the equilibrium state.

Since the FCC structure is symmetrical on the x, y and z directions, the oscillation frequencies of an atom on three directions are the same and can be obtained according to the result of Eq. (7):

$$\omega^{(x)}_{atom-3D} = \omega^{(y)}_{atom-3D} = \omega^{(z)}_{atom-3D} = \sqrt{\frac{4k}{m_{atom}}} \tag{8}$$

For active atoms in molecule regions, their oscillation frequencies are consistent, since the interactions with neighbored atoms should always be considered whether inside the regions or on the interface. However, the oscillation frequencies of nodes inside the mesh and on the coupling interface are distinct on account of the extra interatomic interactions. Due to the fact that the coordinates of nodes on the interface directly affect the distribution of neighbored atoms in molecule regions, the oscillation frequency of nodes on the interface are considered fundamental for synchronizing the convergence rates.

For the oscillations of the node C on the interface, the energy variation should be considered from two aspects: (i) changes in the interatomic distance among the atoms in the cluster containing node C; (ii) changes in the interatomic distance of neighbored atoms on the interface between molecule and cluster regions. To simplify the expressions, it is assumed that the number of FCC cells that can fit to a leg of a tetrahedral element is $n = L_e/\delta_c$, where L_e is the length of the legs of each tetrahedral elements, and δ_c represents the distance of two cells of FCC structure. If a node is disturbed by Δz on the z direction, the distance between two neighbored atoms in the element will increase or decrease by $\Delta z/2n$. Further, considering the mesh division shown in Fig. 7, node C belongs to 12 tetrahedral elements, which contain $8n^3$ atoms in total. As a result, we can calculate the increase of energy in cluster regions:

$$\Delta E^{(z,1)}_{node-3D} = 8n^3 \times \frac{1}{2} \times 8 \times \frac{1}{2} k \left(\frac{\sqrt{2}}{4n} \Delta z \right)^2 = 4nk\Delta z^2 \tag{9}$$

For each atom on the interface whose coordinates variate, the interatomic interactions should be recalculated, and then summarized to obtain a new energy. Here we use the integration in place of summation, since L_e is much larger than δ_c according to our assumptions. In 3D cases, all atoms in triangles that include the node should be considered, thus a surface integral is required. On the interface, all the triangles that contain node C form a hexagon, and the energy variation of atoms on the hexagon should be integrated. Besides, for each atom on the hexagon, the increase of energy is equal to $k\Delta z^2$ when the interatomic distance increases or decreases by Δz on the z direction. And the linear interpolation functions of atomic displacements are $1-|x|/L_e-|y|/L_e$, $1-|x|/L_e$ and $1-|y|/L_e$, with node C as the origin and right angle as the axis. By integrating with respect to the hexagon, we can calculate the increase of energy as follows:

$$\begin{aligned} \Delta E^{(z,2)}_{node-3D} &= k\Delta z^2 \times \frac{1}{\delta_c^2} \left[2 \times \int_0^{L_e} \int_0^{x} \left(1 - \frac{x}{L_e} - \frac{y}{L_e}\right)^2 \mathrm{d}x\mathrm{d}y + 2 \times \int_0^{L_e} \right. \\ &\quad \left. \times \int_x^{L_e} \left(1 - \frac{x}{L_e}\right)^2 \mathrm{d}x\mathrm{d}y + 2 \times \int_0^{L_e} \int_y^{L_e} \left(1 - \frac{y}{L_e}\right)^2 \mathrm{d}x\mathrm{d}y \right] \\ &= \frac{1}{2} n^2 k \Delta z^2 \end{aligned} \tag{10}$$

Similarly, one could calculate the energy variation on the x and y directions. As a consequence, the oscillation frequencies of nodes on three directions can be obtained:

$$\begin{aligned} \omega^{(x)}_{node-3D} = \omega^{(y)}_{node-3D} &= \sqrt{\left(4n + \frac{1}{2}n^2\right) \frac{k}{m_{node-3D}}}, \omega^{(z)}_{node-3D} \\ &= \sqrt{(4n + n^2) \frac{k}{m_{node-3D}}} \end{aligned} \tag{11}$$

where $m_{node-3D}$ represents the effective mass of nodes in 3D cases.

From Eq. (8) and Eq. (11), it is evident that the oscillation frequencies of atoms and nodes differ across three directions. Here, we consider the product of oscillation frequencies on different directions, which corresponds to the determinant of the lattice dynamical matrix [46–48]. Therefore, the relationship of effective masses between atoms and nodes is given through synchronizing their oscillation frequencies:

$$m_{node-3D} = \sqrt[3]{\left(n + \frac{1}{8}n^2\right)^2 \left(n + \frac{1}{4}n^2\right)} m_{atom} \tag{12}$$

Similarly, the relationship of effective masses could be analyzed for 1D or 2D multiscale cases with different lattice configurations, and the results are detailed in Appendix B.

5. Numerical validation

5.1. Structural relaxation of 2D plates

Firstly, the structural relaxation of a 2D sample is validated for the multiscale FIRE algorithm. As shown in Fig. 8 (a), a 2D plate consisted of 250,751 Cu atoms is used for energy minimization in the full atomistic simulation. The lattice structure is hexagonal close-packed (HCP), with the lattice constant of 2.588 Å. In the multiscale system, the molecule regions contain 49,550 atoms, while the cluster regions are divided into 48 triangular elements. The division of two regions is fixed throughout the process of structural relaxation without adaptive transformation. The Lennard-Jones potential $\phi_{Cu-Cu}(r) = 4\varepsilon_{Cu-Cu}\left[(\sigma_{Cu-Cu}/r)^{12} - (\sigma_{Cu-Cu}/r)^6\right]$ is adopted for the atomic interactions, where the parameters $\varepsilon_{Cu-Cu} = 0.4912$ eV and $\sigma_{Cu-Cu} = 2.3276$ Å are used [49]. At the very beginning, a random displacement perturbation ranging from −0.005 to 0.005 Å is applied to each DOFs. Subsequently, the two systems are relaxed through the FIRE algorithm.

As a comparison of efficiency, Table 2 shows the number of force evaluations and computational time by MST and HMCST methods using the original FIRE (m_{node}=m_{atom}) and multiscale FIRE algorithms. For the multiscale FIRE, the relationship of effective mass between atoms and nodes is $m_{node} = 14.4\ m_{atom}$ according to Eq. (14) in Appendix B.

It is observed that HMCST-Original FIRE consumes 4.6 times more iterations than MST, thus costing longer computational time. However, with the multiscale FIRE, the efficiency of HMCST improves by 3.5 times than using the original FIRE, which is also 2.9 times higher than MST. These results indicate the great efficiency improvement for multiscale simulations with the proposed multiscale FIRE algorithm.

5.2. 3D nanoindentation

Here the same 3D nanoindentation configuration in Section 3 is used to further validate the multiscale FIRE algorithm. For the nanoindentation system, the effective node mass can be evaluated as $m_{node} = 35.1\ m_{atom}$ according to Eq. (12). Firstly, the dislocation distribution obtained from adaptive HMCST with multiscale FIRE are illustrated in Fig. 9 (a), which are compared with the results of MST and adaptive HMCST with two original FIRE algorithms in Fig. 3. It can be observed from Fig. 9 (a) that dislocation loops generate and propagate to the boundary of the substrate, which is close to the results of MST. The results indicate the fidelity and reliability of HMCST simulations with the multiscale FIRE algorithm.

Further, the force-depth curves obtained by four different methods are shown in Fig. 9 (b). With the same convergence criterion and threshold, two curves obtained by adaptive HMCST simulations with the original FIRE algorithm show distinctions compared with the MST, and the reasons have been analyzed in Section 3. However, the force-depth curve of HMCST-Multiscale FIRE is more close to that of MST. As a quantitative comparison, the coefficients of quadratic fittings for the MST and adaptive HMCST-Multiscale FIRE are 114.9 and 115.3 nN/nm^2 respectively, indicating the fidelity of the proposed multiscale FIRE

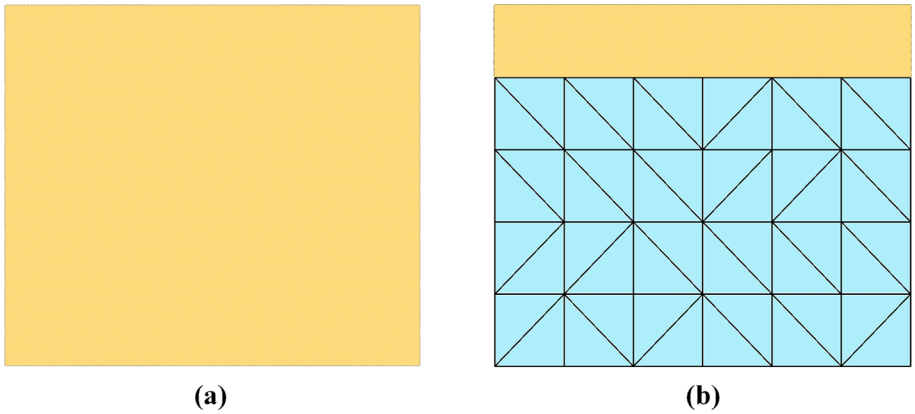

Fig. 8. Configurations of 2D plates for the (a) MST and (b) HMCST methods.

Table 2
Number of force evaluations and computational time of MST and HMCST by different FIRE algorithms.

Method	Number of force evaluations	Computational time (s)
MST-FIRE	137	67.5
HMCST-Original FIRE	633	81.6
HMCST-Multiscale FIRE	**168**	**23.5**

algorithm.

To further demonstrate the computational accuracy of HMCST based on the multiscale FIRE, Fig. 9 (c) shows the average forces of atoms and nodes during the iteration process at the indented depth of 2.2 nm, compared with previous results obtained from two original FIRE algorithms. It is evident that no violent fluctuation occurs in Fig. 9 (c) as in Fig. 5 (a). More importantly, the magnitude of two forces in the results of multiscale FIRE are comparable, thus the molecule and cluster regions could converge with similar accuracy, while the convergence rate of cluster regions in Fig. 5 (b) is obviously slower than that of molecule regions. Therefore, the multiscale FIRE algorithm performs better after synchronizing the convergence rates of molecule and cluster regions.

The computational efficiency of different methods is shown in Table 1. It is obvious that the multiscale FIRE algorithm converges much faster and save a large amount of computational cost compared with other EMAs on adaptive HMCST simulations. The total number of force evaluations of the multiscale FIRE algorithm for HMCST is approximately 4.1 % of CG, 4.3 % of LBFGS and 9.7 %, 37.5 % of the two original FIRE algorithms, and its number of iteration steps for HMCST is compared to that of MST. Attributing to the proper effective mass of nodes by synchronizing the oscillations of atoms and nodes in Section 4.2, the multiscale FIRE algorithm shows much higher efficiency in the adaptive HMCST simulations.

6. Significance of the multiscale FIRE on general multiscale simulations

In Section 5, the proposed multiscale FIRE algorithm has been applied to different multiscale systems to verify its accuracy and efficiency. It is worth noting that the multiscale FIRE algorithm holds significant potential for broader applications within the field of MMMs which are based on energy minimizations, such as QC [6], CADD [16] and CAC [22] methods. Similar to the discussions in Section 4.2, users can perform specific analysis to determine the proper corrected effective mass of nodes based on the practical methods and problems at hand. This step is crucial for ensuring that the multiscale interactions are accurately represented, leading to more reliable simulation outcomes and higher computational efficiency. Furthermore, leveraging the advanced capability of the FIRE method in transition state calculations, especially when integrated with the nudged elastic band (NEB) method, the proposed multiscale FIRE algorithm holds the potential to revolutionize NEB calculations in multiscale methods like QC, CADD, and CAC. This pivotal advancement could catalyze a transformative shift within the computational modeling community, effectively bridging the gaps in different length scales inherent in traditional methods.

In addition, the algorithm could also be served as reference for accelerating simulations on general multiscale problems. When a physical system involves coupling of multiple scales, the problem of inconsistency in convergence may occur, which can be improved by synchronizing the oscillations of DOFs on different scales. As a result, the multiscale FIRE algorithm could be used to not only quasi-static calculations of atomic systems, but also transferred to nano-contact and other types of multiscale problems.

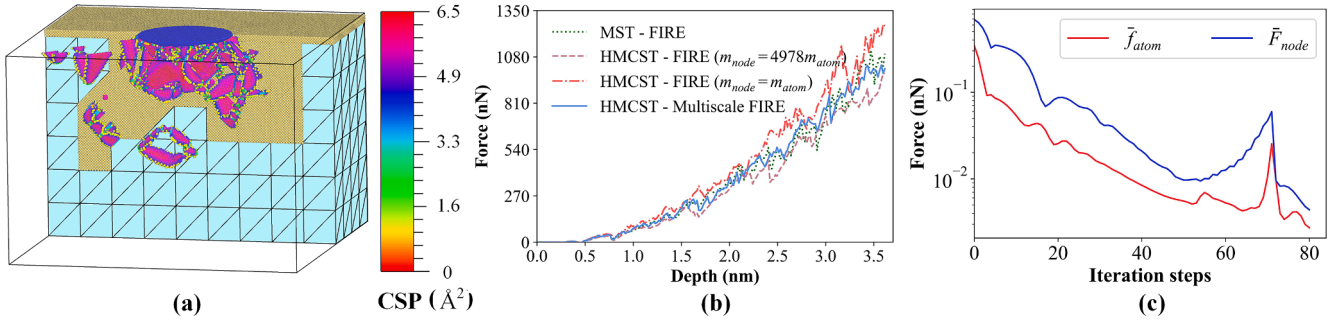

Fig. 9. (a) Dislocation distribution in the nanoindentation systems at the maximum indentation depth obtained from the HMCST-Multiscale FIRE; (b) force-depth curves obtained by the MST, HMCST-Original FIRE and HMCST-Multiscale FIRE methods; (c) average forces of atoms and nodes for the adaptive HMCST simulations with multiscale FIRE algorithm.

7. Summary

In this work, energy minimization algorithms for multiscale simulations with atomistic to continuum coupling are investigated in order to improve the computational efficiency, and a multiscale FIRE algorithm is proposed. The main results and conclusions include:

The use of traditional EMAs in multiscale simulations leads to diminished accuracy and low convergence rate. We simulated the classical nano-indentation process using the HMCST method with coupled atoms and nodes and the MST method with full atoms. The results show that regardless of using traditional CG and LBFGS algorithms or the new FIRE algorithm, the total iteration steps of HMCST is at least 6 times larger than that of MST. This is primarily due to the different length scales of atoms and nodes.

Analysis on the force states of atoms and nodes during the energy minimization process reveals discrepancies in convergence rates of different regions, mainly attributed to the improper step sizes. Further, a 2D quadratic potential function is used to illustrate the importance of synchronizing oscillations of DOFs across different scales. On this basis, we analyze effective mass of nodes to correct the step sizes of atoms and nodes in MMMs. With this key strategy, the convergence rates of regions at different length scales could keep consistent, thus optimal for computational efficiency in energy minimizations of multiscale simulations.

The HMCST using the proposed multiscale FIRE algorithm are applied to the structural relaxation of 2D plates and calculations of 3D nanoindentation systems. The results of 2D simulations indicate the effectiveness of multiscale FIRE for general multiscale optimization problems. The results of 3D nanoindentation show that the computational efficiency of the multiscale FIRE algorithm is 24 times higher than traditional CG and LBFGS algorithms, and 10 times higher than the original FIRE algorithm. In addition, the force states show good consistency of convergence rates between molecule and cluster regions.

In general, the multiscale FIRE algorithm can be not only applied to the computation of MMMs with atomistic to continuum coupling, but also served as a reference for developing novel and efficient minimization algorithms adapted to other types of multiscale simulations.

CRediT authorship contribution statement

Mingjian Tang: Writing – original draft, Visualization, Validation, Software, Methodology, Investigation, Formal analysis, Data curation, Conceptualization. **Fei Shuang:** Writing – review & editing, Supervision, Project administration, Investigation, Conceptualization. **Pan Xiao:** Writing – review & editing, Supervision, Software, Resources, Project administration, Funding acquisition, Conceptualization.

Declaration of competing interest

The authors declare that they have no known competing financial interests or personal relationships that could have appeared to influence the work reported in this paper.

Data availability

Data will be made available on request.

Acknowledgments

This work was supported by the National Natural Science Foundation of China (NSFC) (11790292 and 11672298), the NSFC Basic Science Center Program for "Multiscale Problems in Nonlinear Mechanics" (11988102) and the Strategic Priority Research Program of Chinese Academy of Sciences (XDB0620103).

Appendix A. Computational process of the FIRE 2.0 algorithm for the HMCST method

1: Initialize $\mathbf{x}_{atom}$, $\mathbf{X}_{node}$, $\mathbf{v}_{atom} = 0$, $\mathbf{V}_{node} = 0$, $N_{P>0} = 0$, $N_{P\le 0} = 0$.
2: Define parameters N_{delay}, $N_{P\le 0,\max}$, f_{inc}, f_{dec}, f_α, $\alpha = \alpha_0$, Δt, m_{atom}, m_{node}.
3: **for** $k = 0, 1, 2, \ldots,$ **do**
4: $P = \mathbf{f}_{atom} \bullet \mathbf{v}_{atom} + \mathbf{F}_{node} \bullet \mathbf{V}_{node}$.
5: **if** $P > 0$, **then**
6: $N_{P>0} = N_{P>0} + 1$, $N_{P\le 0} = 0$.
7: **if** $N_{P>0} > N_{delay}$, **then**
8: $\Delta t = \min\{f_{inc}\Delta t, \Delta t_{\max}\}$, $\alpha = f_\alpha \bullet \alpha$.
9: **end if**
10: **else**
11: $N_{P\le 0} = N_{P\le 0} + 1$, $N_{P>0} = 0$.
12: **if** $k \ge N_{delay}$ and $f_{dec}\Delta t \ge \Delta t_{min}$, **then**
13: $\Delta t = f_{dec}\Delta t$.
14: **end if**
15: **if** $N_{P\le 0} > N_{P\le 0,\max}$, **then**
16: break.
17: **end if**
18: $\mathbf{x}_{atom} = \mathbf{x}_{atom} - 0.5\mathbf{v}_{atom}\Delta t$, $\mathbf{X}_{node} = \mathbf{X}_{node} - 0.5\mathbf{V}_{node}\Delta t$, $\alpha = \alpha_0$, $\mathbf{v}_{atom} = 0$, $\mathbf{V}_{node} = 0$.
19: **end if**
20: $\mathbf{v}_{atom} = \mathbf{v}_{atom} + \dfrac{\mathbf{f}_{atom}}{m_{atom}}\Delta t$, $\mathbf{V}_{node} = \mathbf{V}_{node} + \dfrac{\mathbf{F}_{node}}{m_{node}}\Delta t$.
21: **if** $P > 0$, **then**
22: $\mathbf{v}_{atom} = (1-\alpha)\mathbf{v}_{atom} + \alpha\|\mathbf{v}_{atom}\| \bullet \dfrac{\mathbf{f}_{atom}}{\|\mathbf{f}_{atom}\|}$, $\mathbf{V}_{node} = (1-\alpha)\mathbf{V}_{node} + \alpha\|\mathbf{V}_{node}\| \bullet \dfrac{\mathbf{F}_{node}}{\|\mathbf{F}_{node}\|}$.
23: **end if**
24: $\mathbf{x}_{atom} = \mathbf{x}_{atom} + \mathbf{v}_{atom}\Delta t$, $\mathbf{X}_{node} = \mathbf{X}_{node} + \mathbf{V}_{node}\Delta t$.
25: Calculate $E(\mathbf{x}_{atom}, \mathbf{X}_{node})$ and $\mathbf{f}_{atom}$, $\mathbf{F}_{node}$
26: Check the criterion of energy or force. If converged, then break.
27: **end for**

Appendix B. Relationships of effective masses of atom and nodes for 1D and 2D cases

B.1. 1D multiscale cases

In a 1D multiscale system, the atoms are tightly packed in molecule regions, while the cluster regions are divided into several bar elements. Based on the assumptions in Section 4.2, the relationship of effective masses could be obtained as follows after synchronizing the oscillation frequencies:

$$m_{node-1D} = (0.5 + 1/n)m_{atom} \tag{13}$$

where n corresponds to the number of atoms in a 1D element.

B.2. 2D multiscale cases

For the 2D multiscale system, we assume that the atomic configuration is HCP, and the cluster regions are divided into several triangular elements. The relationship of effective masses could be obtained as follows:

$$m_{node-2D} = \sqrt{\left(\frac{3\sqrt{3}}{8} + \frac{n}{12}\right)\left(\frac{3\sqrt{3}}{8} + \frac{n}{3}\right)}m_{atom} \tag{14}$$

where n corresponds to the number of atoms that can fit to a leg of a triangle element.

References

[1] S. Xu, X. Chen, Modeling dislocations and heat conduction in crystalline materials: atomistic/continuum coupling approaches, Int. Mater. Rev. 64 (2019) 407–438, https://doi.org/10.1080/09506608.2018.1486358.

[2] G.D. Manolis, P.S. Dineva, T. Rangelov, D. Sfyris, Mechanical models and numerical simulations in nanomechanics: a review across the scales, Eng. Anal. Bound. Elem. 128 (2021) 149–170, https://doi.org/10.1016/j.enganabound.2021.04.004.

[3] P.R. Budarapu, X. Zhuang, T. Rabczuk, S.P. Bordas, Multiscale modeling of material failure: Theory and computational methods, Advances in applied mechanics 52 (2019) 1–103, https://doi.org/10.1016/bs.aams.2019.04.002.

[4] A.C. To, W.K. Liu, G.B. Olson, T. Belytschko, W. Chen, M.S. Shephard, Y.W. Chung, R. Ghanem, P.W. Voorhees, D.N. Seidman, C. Wolverton, J.S. Chen, B. Moran, A. J. Freeman, R. Tian, X. Luo, E. Lautenschlager, A.D. Challoner, Materials integrity in microsystems: a framework for a petascale predictive-science-based multiscale modeling and simulation system, Comput. Mech. 42 (2008) 485–510, https://doi.org/10.1007/s00466-008-0267-1.

[5] R.E. Miller, E.B. Tadmor, A unified framework and performance benchmark of fourteen multiscale atomistic/continuum coupling methods, Model. Simul. Mater. Sci. Eng. 17 (2009), https://doi.org/10.1088/0965-0393/17/5/053001.

[6] E.B. Tadmor, R. Phillips, M. Ortiz, Mixed atomistic and continuum models of deformation in solids, Langmuir. 12 (1996) 4529–4532, https://doi.org/10.1021/la9508912.

[7] R.E. Miller, E.B. Tadmor, The quasicontinuum method: overview, applications and current directions, J. Comput. Mater. Des. 9 (2002) 203–239, https://doi.org/10.1023/A:1026098010127.

[8] I. Tembhekar, J.S. Amelang, L. Munk, D.M. Kochmann, Automatic adaptivity in the fully nonlocal quasicontinuum method for coarse-grained atomistic simulations, Int. J. Numer. Methods Eng. 110 (2017) 878–900, https://doi.org/10.1002/nme.5438.

[9] V.B. Shenoy, R. Miller, E.B. Tadmor, D. Rodney, R. Phillips, M. Ortiz, An adaptive finite element approach to atomic-scale mechanics - the quasicontinuum method, J. Mech. Phys. Solids. 47 (1999) 611–642, https://doi.org/10.1016/S0022-5096(98)00051-9.

[10] X. Li, P. Ming, On the effect of ghost force in the quasicontinuum method: dynamic problems in one dimension, Commun Comput. Phys. 15 (2014) 647–676, https://doi.org/10.4208/cicp.250213.270813a.

[11] V. Shenoy, V. Shenoy, R. Phillips, Finite temperature quasicontinuum methods, Mater. Res. Soc. Symp. - Proc. 538 (1999) 465–471, https://doi.org/10.1557/proc-538-465.

[12] L.M. Dupuy, E.B. Tadmor, R.E. Miller, R. Phillips, Finite-temperature quasicontinuum: molecular dynamics without all the atoms, Phys. Rev. Lett. 95 (2005) 1–4, https://doi.org/10.1103/PhysRevLett.95.060202.

[13] T. Zhou, X. Yang, C. Chen, Quasicontinuum simulation of single crystal nano-plate with a mixed-mode crack, Int. J. Solids Struct. 46 (2009) 1975–1980, https://doi.org/10.1016/j.ijsolstr.2009.01.010.

[14] I. Ringdalen Vatne, A. Stukowski, C. Thaulow, E. Østby, J. Marian, Three-dimensional crack initiation mechanisms in bcc-Fe under loading modes I, II and III, Mater. Sci. Eng. A. 560 (2013) 306–314, https://doi.org/10.1016/j.msea.2012.09.071.

[15] L.E. Shilkrot, R.E. Miller, W.A. Curtin, Coupled atomistic and discrete dislocation plasticity, Phys. Rev. Lett. 89 (2002) 1–4, https://doi.org/10.1103/PhysRevLett.89.025501.

[16] B. Shiari, R.E. Miller, W.A. Curtin, Coupled atomistic/discrete dislocation simulations of nanoindentation at finite temperature, J. Eng. Mater. Technol. 127 (2005) 358–368, https://doi.org/10.1115/1.1924561.

[17] G.J. Wagner, W.K. Liu, Coupling of atomistic and continuum simulations using a bridging scale decomposition, J. Comput. Phys. 190 (2003) 249–274, https://doi.org/10.1016/S0021-9991(03)00273-0.

[18] D. Qian, G.J. Wagner, W.K. Liu, A multiscale projection method for the analysis of carbon nanotubes, Comput. Methods Appl. Mech. Eng. 193 (2004) 1603–1632, https://doi.org/10.1016/j.cma.2003.12.016.

[19] H.S. Park, E.G. Karpov, K.L. Wing, P.A. Klein, The bridging scale for two-dimensional atomistic/continuum coupling, Philos. Mag. 85 (2005) 79–113, https://doi.org/10.1080/14786430412331300163.

[20] P.R. Budarapu, R. Gracie, S.P.A. Bordas, T. Rabczuk, An adaptive multiscale method for quasi-static crack growth, Comput. Mech. 53 (2014) 1129–1148, https://doi.org/10.1007/s00466-013-0952-6.

[21] S. Wang, L. Zhao, Y. Liu, A concurrent multiscale method based on smoothed molecular dynamics for large-scale parallel computation at finite temperature, Comput. Methods Appl. Mech. Eng. 406 (2023) 115898, https://doi.org/10.1016/j.cma.2023.115898.

[22] Y. Chen, S. Shabanov, D.L. McDowell, Concurrent atomistic-continuum modeling of crystalline materials, J. Appl. Phys. 126 (2019), https://doi.org/10.1063/1.5099653.

[23] H. Wang, M. Hu, M. Xia, F. Ke, Y. Bai, Molecular/cluster statistical thermodynamics methods to simulate quasi-static deformations at finite temperature, Int. J. Solids Struct. 45 (2008) 3918–3933, https://doi.org/10.1016/j.ijsolstr.2007.12.023.

[24] P. Xiao, J. Wang, F.J. Ke, Y.L. Bai, Molecular statistical thermodynamics - a distinct and efficient numerical approach to quasi-static analysis of nanomaterials at finite temperature, Compos. Part B Eng. 43 (2012) 57–63, https://doi.org/10.1016/j.compositesb.2011.04.031.

[25] M. Hu, H. Wang, M. Xia, F. Ke, Y. Bai, Cluster statistical thermodynamics (CST) - To efficiently calculate quasi-static deformation at finite temperature based on molecular potential, Solid Mech. Its Appl. 144 (2007) 163–170, https://doi.org/10.1007/978-1-4020-5624-6_16.

[26] H. Tan, H. Wang, M. Xia, F. Ke, Y. Bai, Self-adaptive molecule/cluster statistical thermodynamics method for quasi-static deformation at finite temperature, Acta Mech. Solida Sin. 24 (2011) 92–100, https://doi.org/10.1016/S0894-9166(11)60011-6.

[27] E. Biyikli, A.C. To, Multiresolution molecular mechanics: implementation and efficiency, J. Comput. Phys. 328 (2017) 27–45, https://doi.org/10.1016/j.jcp.2016.10.010.

[28] O. Alizadeh, S. Mohammadi, The variable node multiscale approach: coupling the atomistic and continuum scales, Comput. Mater. Sci. 160 (2019) 256–274, https://doi.org/10.1016/j.commatsci.2019.01.003.

[29] H. Zhang, H. Li, H. Ye, Y. Zheng, Y. Zhang, A coupling extended multiscale finite element and peridynamic method for modeling of crack propagation in solids, Acta Mech. 230 (2019) 3667–3692, https://doi.org/10.1007/s00707-019-02471-2.

[30] T.G. Kolda, R.M. Lewis, V. Torczon, Optimization by direct search: new perspectives on some classical and modern methods, SIAM Rev. 45 (2003) 385–482, https://doi.org/10.1137/S003614450242889.

[31] E. Bitzek, P. Koskinen, F. Gähler, M. Moseler, P. Gumbsch, Structural relaxation made simple, Phys. Rev. Lett. 97 (2006) 1–4, https://doi.org/10.1103/PhysRevLett.97.170201.

[32] L. Yang, C. Hou, X. Ma, L. Ye, L. Chang, L. Shi, X. He, Structure relaxation via long trajectories made stable, Phys. Chem. Chem. Phys. 19 (2017) 24478–24484, https://doi.org/10.1039/c7cp04838f.

[33] Y. Zhou, M. Moseler, M.H. Müser, Solution of boundary-element problems using the fast-inertial-relaxation-engine method, Phys. Rev. B. 99 (2019) 1–8, https://doi.org/10.1103/PhysRevB.99.144103.
[34] J. Guénolé, W.G. Nöhring, A. Vaid, F. Houllé, Z. Xie, A. Prakash, E. Bitzek, Assessment and optimization of the fast inertial relaxation engine (FIRE) for energy minimization in atomistic simulations and its implementation in LAMMPS, Comput. Mater. Sci. 175 (2020) 109584, https://doi.org/10.1016/j.commatsci.2020.109584.
[35] S. Plimpton, Fast parallel algorithms for short-range molecular dynamics, J. Comput. Phys. 117 (1995) 1–19, https://doi.org/10.1006/jcph.1995.1039.
[36] G. Kresse, J. Furthmüller, Efficiency of ab-initio total energy calculations for metals and semiconductors using a plane-wave basis set, Comput. Mater. Sci. 6 (1996) 15–50, https://doi.org/10.1016/0927-0256(96)00008-0.
[37] J. Stadler, R. Mikulla, H.R. Trebin, IMD: a software package for molecular dynamics studies on parallel computers, Int. J. Mod. Phys. C. 8 (1997) 1131–1140, https://doi.org/10.1142/S0129183197000990.
[38] M.J. Abraham, T. Murtola, R. Schulz, S. Páll, J.C. Smith, B. Hess, E. Lindah, Gromacs: high performance molecular simulations through multi-level parallelism from laptops to supercomputers, SoftwareX. 1–2 (2015) 19–25, https://doi.org/10.1016/j.softx.2015.06.001.
[39] B. Eidel, A. Stukowski, J. Schröder, Accelerated energy-minimization in the quasicontinuum method with application to nanopillar compression, in: COMPLAS XI: proceedings of the XI International Conference on Computational Plasticity: fundamentals and applications, CIMNE, 2011, pp. 360–367.
[40] J.M. Rickman, R. Najafabadi, L. Zhao, D.J. Srolovitz, Finite-temperature properties of perfect crystals and defects from zero-temperature energy minimization, J. Phys. Condens. Matter. 4 (1992) 4923–4934, https://doi.org/10.1088/0953-8984/4/21/008.
[41] Y. Chen, J. Zimmerman, A. Krivtsov, D.L. McDowell, Assessment of atomistic coarse-graining methods, Int. J. Eng. Sci. 49 (2011) 1337–1349, https://doi.org/10.1016/j.ijengsci.2011.03.018.
[42] K. Xiong, X. Liu, J. Gu, Multiscale modeling of nanoindentation-induced instability in FeNi3 crystal, Comput. Mater. Sci. 102 (2015) 140–150, https://doi.org/10.1016/j.commatsci.2015.02.027.
[43] M. Chamani, G.H. Farrahi, Multiscale modeling of nanoindentation and nanoscratching by generalized particle method, J. Mol. Graph. Model. 127 (2024) 108675, https://doi.org/10.1016/j.jmgm.2023.108675.
[44] S.M. Foiles, M.I. Baskes, M.S. Daw, Embedded-atom-method functions for the fcc metals Cu, Ag, Au, Ni, Pd, Pt, and their alloys, Phys. Rev. B. 33 (1986) 7983–7991, https://doi.org/10.1103/PhysRevB.33.7983.
[45] C.L. Kelchner, S.J. Plimpton, J.C. Hamilton, Dislocation nucleation and defect structure during surface indentation, Phys. Rev. B. 58 (1998) 11085–11088, https://doi.org/10.1103/PhysRevB.58.11085.
[46] M. Born, K. Huang, Dynamical Theory of Crystal Lattices, Oxford University Press, London, UK, 1954.
[47] C. Kittel, R.W. Hellwarth, Introduction to solid state physics, Phys. Today. 10 (1957) 43–44, https://doi.org/10.1063/1.3060399.
[48] C.J. Kimmer, R.E. Jones, Continuum constitutive models from analytical free energies, J. Phys. Condens. Matter. 19 (2007), https://doi.org/10.1088/0953-8984/19/32/326207.
[49] F. Shuang, P. Xiao, F. Ke, Y. Bai, Efficiency and fidelity of molecular simulations relevant to dislocation evolutions, Comput. Mater. Sci. 139 (2017) 266–272, https://doi.org/10.1016/j.commatsci.2017.07.044.